Hindawi
Journal of Chemistry
Volume 2022, Article ID 3476954, 15 pages
https://doi.org/10.1155/2022/3476954

Research Article

Study of Synthesis, Characterization, DFT, and In Vitro Biological Activity of Cu(II), Co(II), and Fe(II) Metal Complexes Based on Heterocyclic Azo Pyrazole Dye Ligand

Albandari Alkurdi, Mutlaq AlJahdali, and Abdulmohsen Alshehri

Department of Chemistry, King Abdulaziz University, P.O. Box 80200, Jeddah 21589, Saudi Arabia

Correspondence should be addressed to Albandari Alkurdi; b.f.h.alkurdi@gmail.com

Received 8 November 2022; Revised 16 November 2022; Accepted 24 November 2022; Published 16 December 2022

Academic Editor: Liviu Mitu

A new azo dye ligand was synthesized by coupling 5-amino-3-methyl-1-phenylpyrazole with a diazonium ion of 2-amino-1-naphthalene sulfonic acid. Its Co(II), Fe(II), and Cu(II) complexes were also synthesized. This ligand and its complexes were characterized based on elemental analysis, IR, ^{1}H NMR, UV-vis spectra, and thermogravimetric analysis. The data showed that the proposed complexes have an octahedral geometry around the central metal ion. The nonelectrolytic nature of the complexes was confirmed by molar conductance measurement. X-ray powder diffraction indicates that Co(II) and Fe(II) complexes are amorphous in nature, whereas the Cu(II) complex has crystalline and amorphous phases. The bond strength and molecular stability between the interaction of metal ions and the ligand were investigated by density functional theory (DFT). The in vitro antibacterial activity of the ligand and complexes was tested against two Gram-positive bacteria (*Bacillus subtilis* and *Staphylococcus aureus*) and two Gram-negative bacteria (*Escherichia coli* and *Neisseria gonorrhoeae*) and a fungus (*Candida albicans*). The Cu(II) complex exhibited a high antimicrobial effect against all tested microorganisms. The DNA fragmentation percentage and cytotoxic activity against human liver cancer cells (HepG2) were evaluated. All tested compounds showed potential anticancer activity, and the Co(II) complex showed better activity results than the other tested compounds, with $IC_{50} = 19.55\,\mu g/mL$.

1. Introduction

The synthesis of a new ligand with distinctive characteristics and novel reactivity is possibly the most significant step in the evolution of metal complexes. The heterocyclic ligand that contains the pyrazole ring system plays an important role in various pharmacological and medicinal compound syntheses [1]. Furthermore, the survey of the literature revealed that organic acids are a major class of organic molecules with a general structure R-COOH (including fatty acids and amino acids), such as carboxylic acids, amino acids, and naphthoic acids. These organic acids play an important role due to their biological activities and therapeutic applications [2, 3].

Azo dyes are the largest and most famous coordination compounds, exhibiting biological activities against bacteria and fungi [4]. Azo dyes are organic compounds bearing the functional group R-N = N-R', in which *R* and R' are usually aryls [5]. An azo coupling reaction is an organic interaction in which a diazonium salt and a coupling agent are combined using a metal catalyst to produce aromatic azo compounds [6]. This reaction is commonly used in the industrial production of dyes and lake pigments. In the coupling reaction, diazonium ions act as electrophiles with activated aromatics, such as aniline or phenols. The substitution reaction usually occurs at the para position; however, if the para position is occupied, the ortho position is preferred. Moreover, the coupling reaction must occur under slightly acidic or neutral conditions, since the reaction does not occur at a considerably low pH [7].

In the present study, a new bi-heterocyclic azo dye (AMePhPNA) was synthesized using 5- amino-3-methyl-1-

phenylpyrazole as the diazo component and 2-naphthoic acid as the coupling component, due to their low cost, brilliant color, good stability, easy preparation, and pharmacological and industrial importance [8]. The coordination behavior of the azo dye-based ligand toward Cu(II), Co(II), and Fe(II) ions was investigated, and the results were obtained by physical properties, such as thermal analyses, infrared (FT-IR), UV-visible spectroscopy, X-ray powder diffraction (XRD), and DFT calculations. Moreover, the compounds were tested for their in vitro antimicrobial and antioxidant activities, and DNA fragmentation was identified in liver cancer cells (HepG2).

2. Experiment

2.1. Materials and Methods. All chemicals, reagents, solvents, and metal salts used were of analytical grade.

The percentage compositions of C, H, N, and M were determined using a Leco CHNS-932 analyzer. FT-IR spectra (KBr) were recorded at 4000–400 cm^{-1} on a Bruker Alpha FT-IR spectrophotometer. ^1H NMR spectra were recorded on a JEOL instrument using 500 MHz, DMSO-d6 at 25°C. UV-vis spectra were scanned at 200–800 nm on a Shimadzu 1600 spectrometer using DEMSO as the solvent. Melting points of the compounds were determined on an electrothermal apparatus using open capillary tubes and reported without correction. Magnetic moments were recorded by Gouy's method at room temperature using a Johnson Matty magnetic susceptibility. Differential thermal analysis (DTA)/thermogravimetric analysis (TGA) of the metal complexes was performed in a nitrogen atmosphere from room temperature (25°C) to 800°C using a Shimadzu TG-50 H thermal analyzer. The morphology of the metal complexes was determined by scanning electron microscopy (SEM) images obtained using a JEOL JSM-5410 microscope. X-ray powder diffraction patterns were recorded using a PW3050/60 X-ray diffractometer with CuKα radiation ($\lambda = 1.541$ nm) in the 2θ range of 10°–80°.

2.2. Synthesis of the Ligand. The 1-((5-amino-3-methyl-1-phenyl-1*H*-pyrazol-4-yl) diazenyl)-2-naphthoic acid azo dye ligand (HL) was synthesized by applying the diazo coupling reaction [9]. A diazonium solution was prepared by dissolving 5-amino-3-methyl-1-phenylpyrazole (1.73 g, 0.01 mol) in a 50 mL mixture solution (4 mL HCl distilled water/4 mL HCl). The resultant mixture was cooled down to 0–5°C. A solution of $NaNO_2$ (0.69 g, 0.01 mol) in 30 mL of H_2O was added to this mixture dropwise at 0–5°C and was continuously stirred for 25 min to form the diazo compound (solution A), as shown in (Scheme 1). The aqueous solution B of 2-amino-1-naphthalenesulfonic acid (2.23 g, 0.01 mol) was dissolved in 50 mL of ethanol and strong alkaline sodium hydroxide (0.84 g, 0.01 mol) at 0–5°C. Solution B was added dropwise with contentious stirring of solution A for 30 min at 0–5°C in an ice bath. It was acidified with dilute HCl at pH 6.0. The brown precipitate of the HL ligand was filtered off and washed several times with distilled water and ethanol. The crystals were dried for 24 h at 25°C.

2.3. Synthesis of Metal Complexes. The transition metal complexes were synthesized by dissolving 0.001 mol of metal chloride ($CuCl_2.2H_2O$ [0.170 g], $CoCl_2.6H_2O$ [0.129 g], and $FeCl_2{\cdot}4H_2O$ [0.198 g]) in 45 mL of hot phosphate buffer solution at pH 6.0. The solution was then added dropwise to a hot ethanolic solution (45 mL) containing 1 mM of the prepared ligand HL. The resulting solution was heated to 70°C for 30 min. The precipitate was filtered off and washed with distilled water and warm ethanol. The obtained products were desiccated in a vacuum over $CaCl_2$ (anhydrous) [10].

3. Biological Studies

3.1. Antimicrobial Test. The compounds were screened in vitro for antimicrobial properties. The agar plates with bacteria were incubated at 35–37°C for 24–48 h, whereas the agar plates with fungi were incubated at 25°C for 48 h [11]. Standard disks of ampicillin (antibacterial agent) and amphotericin (antifungal agent) served as positive controls for antimicrobial activity; however, filter disks impregnated with 10 μL of DMS as negative controls. In brief, 100 μL of the test bacteria/fungi were grown in 10 mL of fresh media until they reached a count of approximately 10^8 cells/mL for bacteria and 10^5 cells/mL for fungi. Approximately 100 μL of microbial suspension was spread on agar plates corresponding to the broth in which they were maintained [12, 13].

3.2. Cell Viability by MTT Assay. The cytotoxic evaluation of the azo ligand and its complexes was conducted using the MTT assay [14]. Approximately 1×10^5 cells/mL HepG2 (100 μL/well) were plated in a 96-well plate and incubated at 37°C for 24 h to develop a complete monolayer sheet. The media were aspirated, and the cells were washed with phosphate buffer saline (5 mg/mL). The plates were then kept in 5% CO_2 at 37°C for 1–5 h. After incubation, the culture medium was removed, and 20 μL of MTT solution was added to each well. DMSO (200 μL) was then added, and the plates were incubated for 5 min. Cell viability was measured using spectrophotometry at a wavelength of 560 nm and a subtracted background of 620 nm. HepG2 cells were treated with different concentrations of compounds (3.125, 6.25, 12.5, 25, 50, and 100 μg/mL) for 24 h [15].

3.3. DNA Fragmentation Assay. The percentage of DNA fragmentation was estimated using the diphenylamine (DPA) assay [16]. HepG2 cells (5×10^5 cells/mL) were cultured and inserted in labeled tubes in a complete RPMI medium, which was centrifuged at $20 \times g$ at 4°C for 10 min. After centrifugation at $200 \times g$, the pellet was resuspended in 1 mL of TTE solution (TE buffer at pH 7.4 with 0.2% Triton X-100 stored at 4°C), and 1 mL of 25% trichloroacetic acid (TCA) was transferred in new conical tubes, followed by incubation overnight at 4°C. The DNA was then hydrolyzed by adding 160 mL of 5% TCA to each tube and heating at 90°C for 15 min. Approximately 320 mL of fresh DPA solution was added to each tube, which was then vortexed. The

Table 1: Physical properties and elemental analytical data of the azo dye ligand and its metal complexes.

Comp.	Molecular formula	Color M.wt. (g/mol)	m.p. °C	Elemental analysis (%) (found) calcd C%	H%	N%	M%	Λ_m ($\Omega^{-1}cm^2mol^{-1}$)	μ_{eff} (B.M)
(HL)	$[C_{21}H_{17}N_5O_2]$	Brown (371)	256	67.91 (67.87)	4.61 (4.60)	18.86 (18.82)	—	24	—
Cu(II) L	$[C_{21}H_{19}Cl_2CuN_5O_3].H_2O$	Brown (523)	>300	48.15 (48.13)	3.66 (3.71)	13.37 (13.34)	12.13 (11.84)	30	1.76
Co(II) L	$[C_{21}H_{19}Cl_2CoN_5O_3].H_2O$	Blue (523)	>300	48.58 (49.05)	3.69 (3.43)	13.49 (13.23)	11.35 (10.68)	41	4.68
Fe(II)L	$[C_{21}H_{19}Cl_2FeN_5O_3].H_2O$	Pale- yellow (516)	>300	48.87 (48.84)	3.71 (3.23)	13.57 (13.14)	10.82 (10.49)	28	5.15

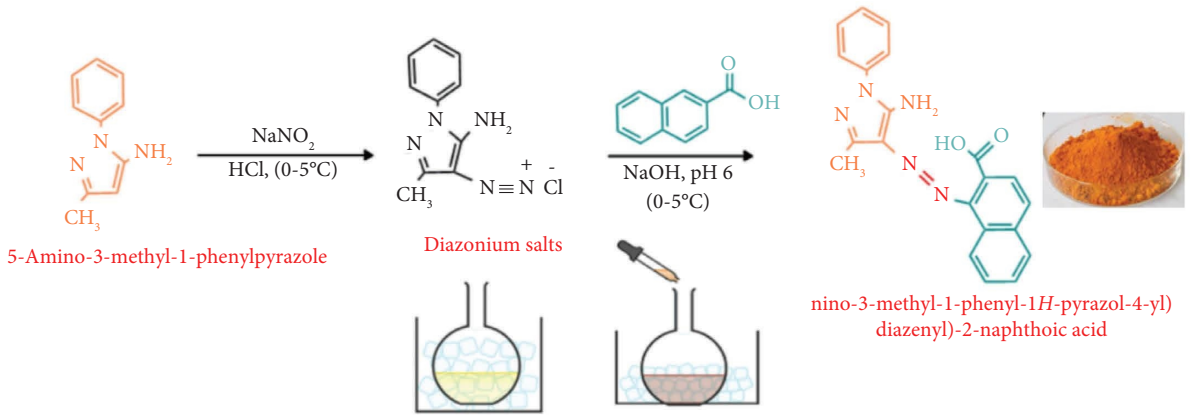

Scheme 1: Synthesis of heterocyclic azo dye ligand (AMePhPNA).

color was allowed to develop by heating at 37°C for 4 h or overnight at room temperature. Two 200 mL aliquots of the colored solution were transferred from each tube to a well of a 96-well microtiter plate. The optical density was determined at 600 nm; however, wavelengths from 560 nm to 620 nm were also considered. The percentage of fragmented DNA was calculated as follows:

$$\%\text{fragmented DNA} = \frac{(S+T)}{(S+T+B)} \times 100, \quad (1)$$

where S, T, and B are the optical densities (OD 600) of fragmented DNA in the S, T, and B fractions, respectively [17].

4. Results and Discussion

4.1. Elemental Analysis and Molar Conductivity Studies. The ligand (AMePhPNA) was prepared by the diazotization coupling reaction of 5-amino-3-methyl-1-phenylpyrazole and 2-amino-1-naphthalenesulfonic acid in a 1 : 1 molar ratio. The results of the elemental analysis (C, H, N, and M) are in a good agreement with those required by the proposed formula, which are apparent in Table 1. The prepared NNO doner azo dye ligand is stable at room temperature, brown in color, and soluble in dimethyl formamide and DMSO. The molar conductance values of the complexes in DEMSO are in the range values ($\Lambda M = 24$–41 ohm^{-1}cm^{2}mol^{-1}), indicating that the complexes are nonelectrolytic in nature [18]. The proposed structure of the Cu(II), Co(II), and Fe(II) complexes is shown in Figure 1 [19].

4.2. Electronic Spectra and Magnetic Properties. The electronic absorption spectra of the prepared azo dye and its complexes were conducted in DMSO, and the data are represented in Figure 2. The diffuse reflectance spectrum of the free ligand displays two main peaks at 42.194 cm^{-1}, and 40.816 cm^{-1} which are attributed to the (π–π^*) electronic transition of the conjugated (C=C) in the aromatic rings and (C=O) of carboxylic acid group. Another band was observed at 29.240 cm^{-1}, which is attributed to the (π–π^*) electronic transition of the (N=N) azo group. These bands are shifted to high or low wavelengths due to the coordination of the ligand with the metal ions.

The Cu(II) complex presented an absorption band in the UV range 43478–41494 cm^{-1}, which was assigned to ligand to metal charge transfer transition (LMCT). The octahedral geometry of the Cu(II) ion is supported by the observed value of the magnetic moment (1.76 BM) [20]. The magnetic moment value of Co(II) was 4.68 BM, suggesting an octahedral environment of the Co(II) ion in the complex. The electronic spectrum of the complex showed one broad band at 19.569 cm^{-1} which can be assigned to d-d transitions [21]. The electronic spectrum of the Fe(II) complex shows an absorption band at 32.787 cm^{-1} which is caused by $\pi \longrightarrow \pi^*$ intraligand transition. Although the spectrum displays another two weak bands at 31.847 and 20.161 cm^{-1} attributed to

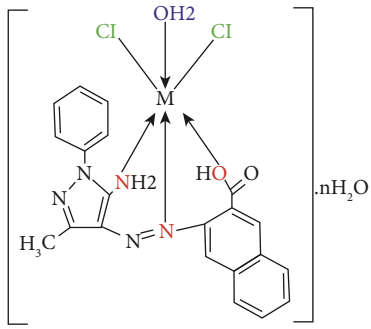

Figure 1: The proposed structure of the metal complexes (M = Cu(II), Co(II), and Fe(II)).

the electronic transition $^5Eg \longrightarrow {}^5T_2g$. The magnetic moment value of 5.15 BM was an additional evidence for an octahedral structure around the metal center [22].

4.3. IR Spectral Studies and the Mode of Bonding. The infrared spectra of the free azo dye ligand were compared with the metal complexes to identify the atoms that participate in the complexation (Table 2; Figure 3). The IR spectrum of the free ligand shows two stretching vibration bands at 3,430–3,305 cm^{-1} due to γ_{asym} (NH_2) and γ_{sym} (NH_2), and the γ (CH_3) stretching vibrations in the region of 2,848–3,118 cm^{-1} both appear as broad peaks of the O-H stretching band that overlap this region [23]. In addition, the strong vibration bands between 1691 and 1656 cm^{-1} are attributed to the stretching vibrations γ (C=O) and γ (C=C), respectively [24]. The vibration of the –N=N– azo group is found at 1,473 cm^{-1} [25, 26]. The IR spectra of all metal complexes display medium broad bands approximately at the 2,476–3,655 cm^{-1} regions, confirming the presence of a coordinated water molecule in the structure of the metal complex. After coordination between the ligand and its Co(II), Co(II), and Fe(II) metal ions, the γ (C=O) was shifted to a low frequency and was observed at 1,622, 1,627, and 1,615 cm^{-1}, respectively, indicating that the coordination occurred through the oxygen of carbonyl [27]. Moreover, the γ (N=N) and γ (NH_2) stretching bands are shifted toward a lower frequency compared with the free ligand, supporting the involvement of one of the azo nitrogen atoms and amino groups in coordination with metal ions. New weak bands were found; these bands have never been observed in the free HL spectrum, which corresponds to γ (M-O), γ (M-N), and γ (M-Cl) stretching [28]. In addition, the IR spectral studies concluded that the HL ligand acts as an NNO-tridentate ligand with three binding sites via the nitrogen atom of the amino group γ (N-H_2), the oxygen atom of the carboxylic group γ (OH), and the nitrogen atom of the azo group γ (N=N).

4.4. ^1H NMR Spectra. The proton NMR spectra of the synthesized azo dye ligand and its Cu(II) complex were recorded in DMSO-d_6 solution as a solvent at room temperature (Figure 4). The three protons signal of the (CH_3) group in the (HL) free ligand appears at 2.0 ppm. Also, the spectrum showed multiple peaks in the range of 7.4–7.9 ppm due to an aromatic ring proton of the ligand. The signal at δ 8.5 ppm may be assigned to the O-H proton in the carboxylic group.

In the ^1H NMR spectrum of the Cu(II) complex, the aromatic protons resonated moved to upfield (~0.2 ppm) due to coordination. While the signal of OH groups shifted downfield (~2.0 ppm), which indicates the bonding of OH group to metal ion. However, the signals of NH_2 are not observed due to the interaction with the solvent DMSO-d^6 [29].

4.5. Thermal Studies. The TGA and DTA studies of the complexes were performed at 0–800°C. The thermal decomposition data of the metal complexes are displayed in Table 3 and Figure 5. The results are in good agreement with the theoretical formula suggested by the elemental analyses.

The TG/DTG curves of the Cu(II) complex were decomposed in two steps. The first step occurred within the temperature range of 64–168°C, which is attributed to the 3½ H_2O lattice water loss. The second step occurred at the temperature range of 173–624°C, with the maximum temperature at 520°C due to 87.0% (calcd. 87.8%) weight loss of two moles of chlorine atoms, one molecule of coordinated water, and the $C_{21}H_{17}N_5O_2$ ligand, leaving CuO as the residue. The thermal decomposition of Co(II)L showed the complete decomposition of the organic ligand in one step, two chlorine atoms, 1 H_2O (lattice), and coordinated H_2O at the temperature range of 40–669°C, with a total 92.6% weight loss (calcd. 92.1%). The thermogram of the Fe(II) complex, the initial weight loss of 10.3% (calcd. 10.4%) occurred at the temperature range of 51–193°C, with DTA_{max} at 99.9°C, due to the loss of $2H_2O$ lattice water molecules and a mole of coordinated water. The second step occurred within a temperature range of 194–649°C, which signifies 85.7% (calcd. 86.0%) loss of 2Cl atoms and ligand molecules, leaving iron oxide as a residue.

4.6. Morphological Behavior. The morphological behaviors of the metal complexes of the azo dye were characterized by XRD measurements and SEM. The X-ray patterns for all samples were recorded between 2θ, ranging from 10° to 80° using the CuKα radiation ($\lambda = 1.540$ Å). Interplanar spacing or d-spacing was calculated using Bragg's law $n\lambda = 2d\sin\Theta$, where Θ is the diffraction angle [30]. The lattice parameters were performed using the Bruker EVA software (Bruker package software). The powder diffraction data 2Θ values are shown in Figure 6. The crystallite size (ξ) of the Cu(II) complex was estimated using the Scherer method, as shown in the following equation [31]:

$$\xi = \frac{K\lambda}{\beta \cos\theta}. \quad (2)$$

The equation uses the reference K, which is the Scherer constant (0.95), β is the full-width peak at half-maximum, and θ is the Bragg diffraction angle. The XRD reflections of

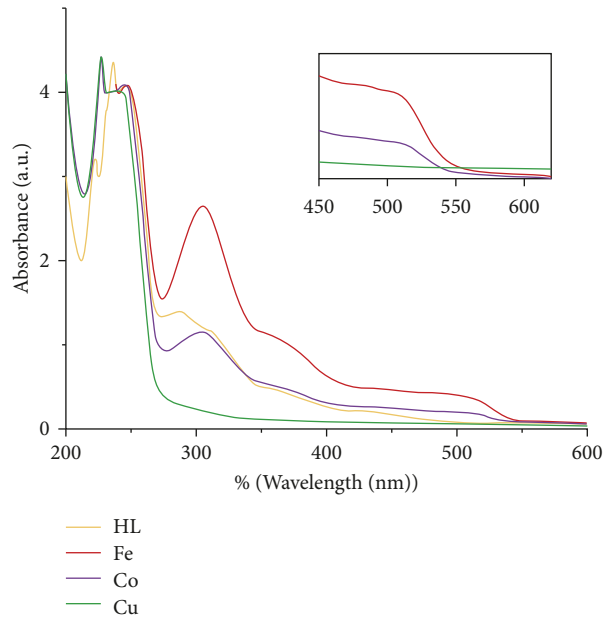

Figure 2: UV-vis absorption spectra of the azo dye ligand (HL) and its Cu (II), Co(II), and Fe(II) metal complexes in DMSO.

Table 2: Important FT-IR spectral bands (cm^{-1}) of the HL ligand and its complexes.

Compound	γ (N-H)	γ (C=O)	γ (C=C)	γ (C=N)	γ (N=N)	γ (C-OH)	γ (M-N)	γ (M-O)	γ (M-Cl)
[HL]	3305–3434	1691	1656	1551	1473	1235	—	—	—
[Cu(II)L]	3232–3340	1622	1591	1503	1386	1286	551	619	502
[Co(II)L)]	3244–3392	1627	1595	1501	1382	1289	561	598	439
[Fe(II)L]	3094–3675	1615	1563	1474	1409	1241	543	595	452

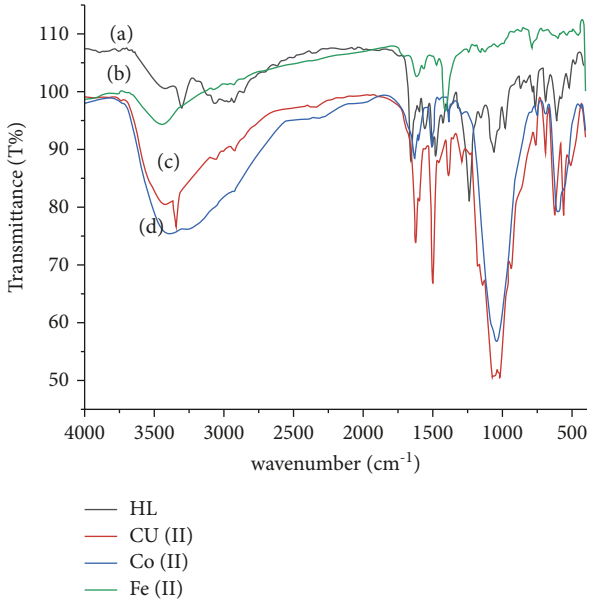

Figure 3: IR spectra at the range 400–4000 cm^{-1} for the (HL) ligand and its metal complexes. (a) HL. (b) Fe(II)L. (c) Cu(II)L. (d) Co(II)L.

the Cu(II) complex show a mixture of crystalline and amorphous phases, as it lacks sharp peaks at maxima $2\Theta = 29.88^{\circ}$. The CuO phase was a monoclinic system at a room temperature, with lattice parameters $a = 4.67$ Å, $b = 3.45$ Å, $c = 5.12$ Å, $\alpha = 90^{\circ}$, $\beta = 98^{\circ}$, $\gamma = 90^{\circ}$, and volume = 81.94 $Å^3$. The value of δ was calculated and was 76 nm. By contrast, crystalline peaks were not observed in the Co(II) and Fe(II) complexes, indicating the amorphous nature of the tested complexes, which could reflect the immeasurably minute sizes of the aggregated particles within the nanosize range.

The surface morphology of the Co(II) complex was investigated using a scanning electron microscope. The SEM images were recorded at different magnifications at an acceleration voltage of 20 kV. The images show that these particles have diameters of 3–20 μm. However, the structural morphology consists of a foam-like shape, as shown in Figure 7.

5. Computational Studies

5.1. Energy and Geometry Optimization. The HyperChem 8.0 program was used for the optimization calculations of the free ligand and its metal complexes. The optimized geometries round the coordination sphere of the free ligand HL and its corresponding complexes are shown in Figure 8. All bond lengths and bond angles of the prepared compounds were calculated, and the values suggest the octahedral geometry around the metal ions as shown in Table 4. A slightly longer bond is between C9-C40 and C17-C18 in the metal complexes compared to the free

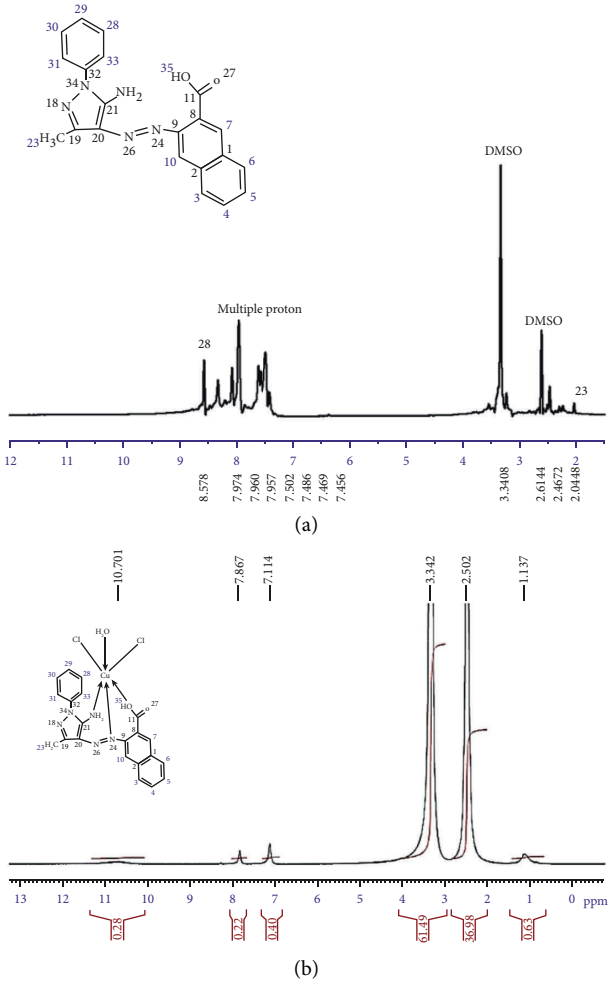

Figure 4: 1H-NMR chemical shifts of compounds (ppm, 500 MHz, DMSO-d6 solutions, room temperature) for (a) HL ligand and (b) Cu(II)L.

Table 3: Thermogravimetric analysis (TGA/DTA) data of the Cu(II), Co(II), and Fe(II) complexes.

Compound	Step	Temp. range °C	DTA_{Max} °C	Total weight loss estimated (calcd.), %	Decomposition assignment	Residual
Cu(II)L	1st	64–168	80.4	12.1 (12.0)	Loss of 3½ H_2O (lattice)	CuO
	2nd	173–624	520	87.0 (87.8)	Loss of 2Cl + 1H_2O (coord.water) + $C_{21}H_{17}N_5O_2$ ligand	
Co(II)L	1st	40–669	400	92.6 (92.1)	Loss of 1H_2O (lattice) + 1H_2O (coord.water) + 2Cl + $C_{21}H_{17}N_5O_2$ ligand	¼ Co_2O_2
Fe(II)L	1st	51–193	99.9	10.3 (10.4)	Loss of 2H_2O (lattice) + 1H_2O (coord.water)	FeO
	2nd	194–649	524.4	85.7 (85.6)	Loss of 2Cl + $C_{21}H_{17}N_5O_2$ ligand	

ligand by 0.01–0.39 Å during the complexation process. The bond length of C17-N27 in case of free ligand was decreased by 0.01–0.04 Å, while C17-N27 is shortest in the case of metal complexes of ≈0.01–0.05 Å. In the case of Fe(II) complex, the bond length M-O is the longest and shortest in the case of Cu(II) complex with a difference of 0.12 Å (6%). Moreover, the bond angles C36-O37-H45 and O37-C36-O38 were significantly changed in the metal case compared to the free ligand by 0.99–4.77° and 1.31–8.24° upon coordination. The value of the bond angle C14-C16-N19 was decreased by 2.82, 2.52, and 4.7°. The calculated bond angles around the central metal ion suggested the regular octahedral geometry for copper (II), cobalt (II), and iron (II) complexes [32].

The quantum chemical parameters such as electrophilicity (ω), global hardness (η), global-softness (s), electronegativity (x), and chemical potential (μ) have been estimated depending on the energy gaps between the two molecular orbitals of the highest occupied molecular orbital energy (EHOMO) and the lowest unoccupied molecular

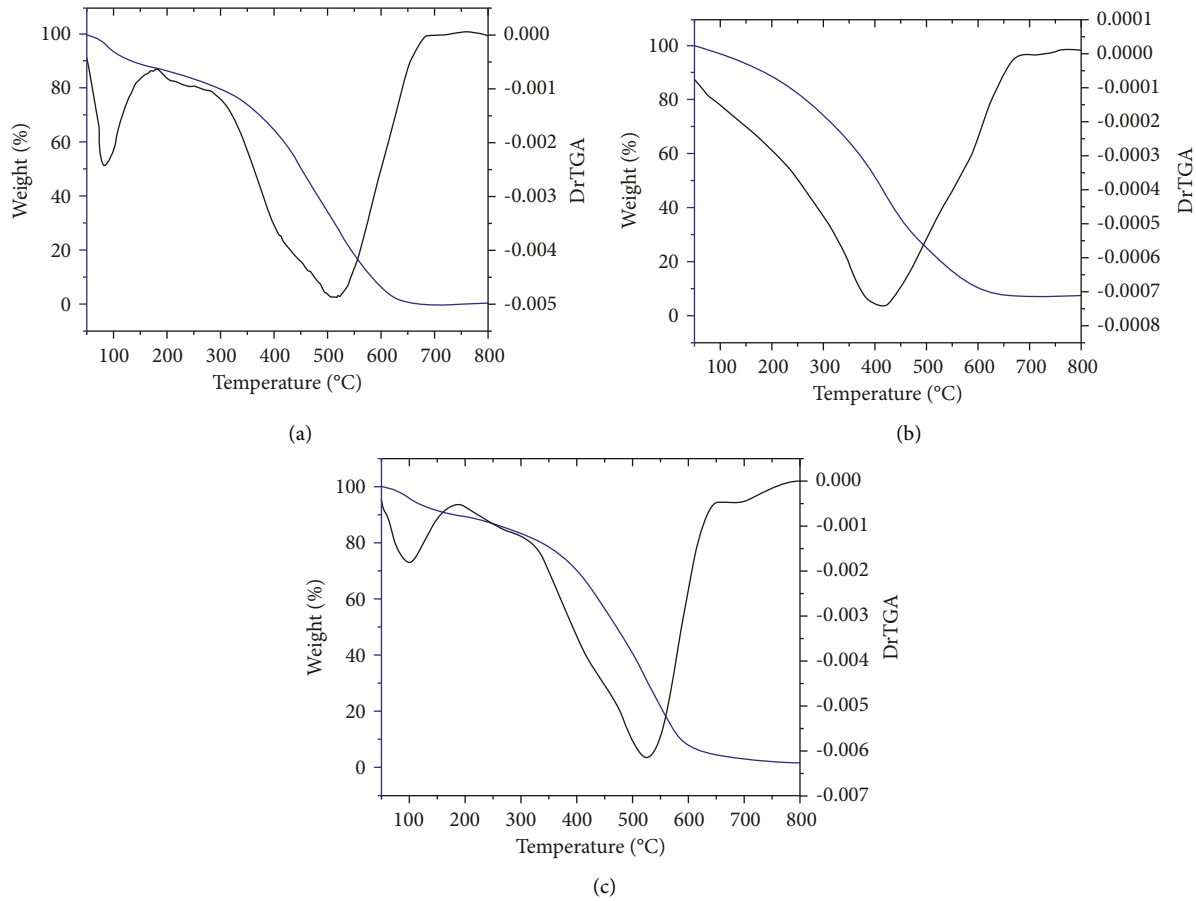

Figure 5: Thermal analysis (TGA/DTA) patterns for the (a) Cu(II), (b) Co(II), and (c) Fe(II) complexes.

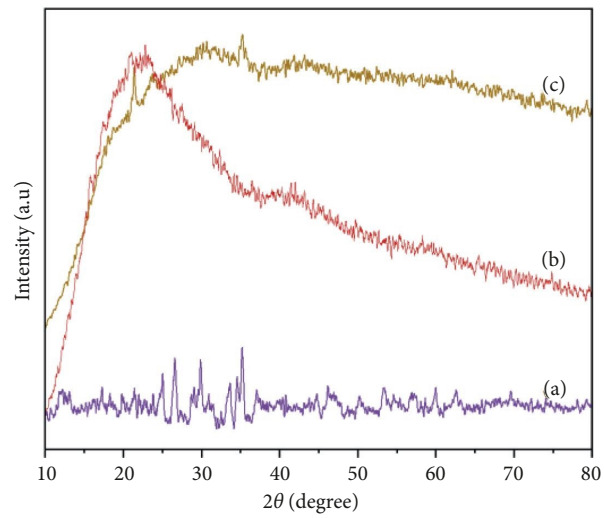

Figure 6: X-ray diffraction patterns of (a) Cu(II), (b) Co(II), and (c) Fe(II) complexes.

orbital energy (ELUMO), which are presented in Figure 9 and Table 5. The energy gap and the parameters were calculated by known equations:

$\Delta\mathbf{E} = (E_{\mathrm{LUMO}} - E_{\mathrm{HOMO}})$, $(\mu) = (E_{\mathrm{HOMO}} + E_{\mathrm{LUMO}})/2$, $(\eta) = (\mathrm{IP} - \mathrm{EA})/2$, $(\sigma) = 1/2\eta$, $(\omega) = \mu^2/2\eta$, $(\chi) = (\mathrm{IP} + \mathrm{EA})/2$, where $\mathrm{IP} = -E_{\mathrm{HOMO}}$, and $\mathrm{EA} = -E_{\mathrm{LUMO}}$.

The negative values of the energy gap ΔE, showing that all investigated compounds are stabilized [33, 34]. Moreover, the results showed that all metal complexes exhibited smaller values of the energy gap than the free ligand, which indicate the greater biological reactivity than the ligand. The global electrophilicity index (ω) of the free

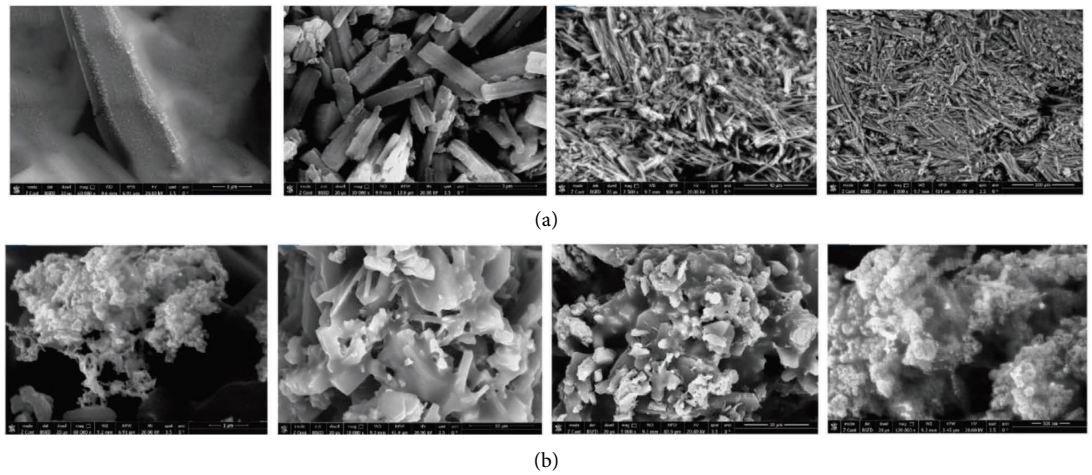

(a)

(b)

Figure 7: Scanning electron micrograph images of the (a) Cu(II)L and (b) Co(II)L complexes.

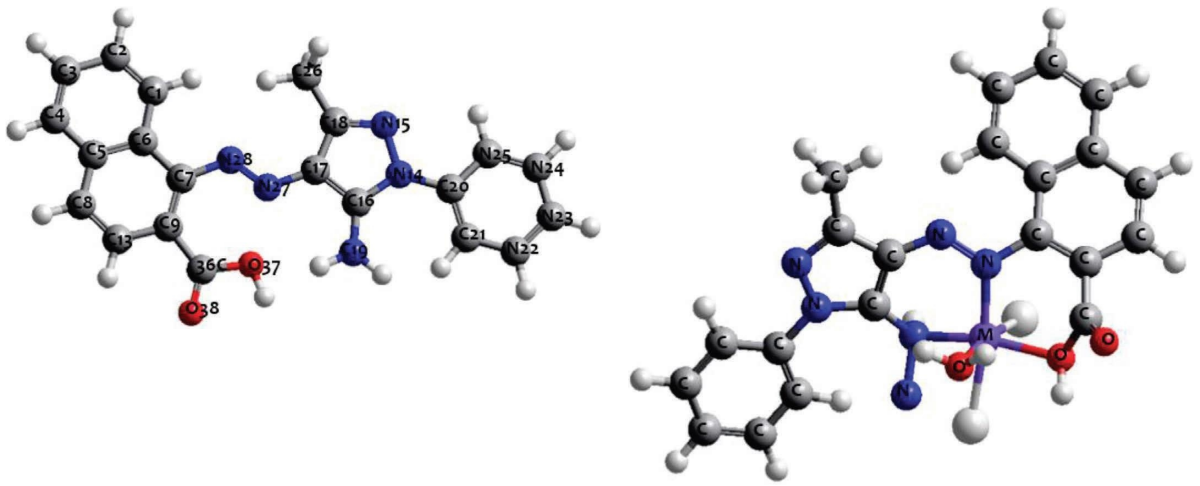

(a) (b)

Figure 8: (a) Optimized geometry of the HL ligand atom numbering. (b) Optimized geometry of the complex where M is the metal atom Cu(II), Co(II), and Fe(II).

ligand has a small value (10.84 eV) compared to the values in metal complexes, indicating the weak electrophile. Furthermore, the electronegativity (χ) of a molecule measures the atom's ability to attract electrons from a neighboring atom to which it is bonded. The calculation of absolute hardness values (η) is useful to measure the stabilization in energy and reactivity for molecular compounds, it could be arranged as follows: HL > Co(II) > Cu(II) > Fe(II) [35].

5.2. Antibacterial Study. The agar diffusion method was conducted to determine the in vitro antimicrobial and antifungal properties of HL and its metal complexes against two gram-positive bacteria, *Bacillus subtilis* and *Staphylococcus aureus*, two gram-negative bacteria, *Neisseria gonorrhoeae* and *Escherichia coli*, and a fungus, *Candida albicans* [36]. The results show that the zone of inhibition (mm) has a larger value for all complexes compared to the free ligand, indicating high effectivity against bacterial and fungal strains, as shown in Figure 10. The higher activity of complexes can be explained by Overtone's concept and Tweedy's chelation theory. The polarity of the metal ion is reduced because of the partial sharing of its positive charge with the donor groups and possible π-electron delocalization over the entire chelate ring [37]. Moreover, other factors affect the activities of the complexes, such as coordination sites, size, concentration, geometry, structure, and hydrophobicity. The Cu(II)L complex shows higher antimicrobial activity than the other compounds, which may be attributed to their particle size and metal ion size [38]. However, the antimicrobial activity of the complexes is lower than that of standard drugs. The zone inhibition values (area in mm) are presented in Table 6.

5.3. Anticancer Activity. The in vitro cytotoxic effects of the AMePhPNA ligand and its Cu(II), Co(II), and Fe(II) complexes were evaluated on a human tumor cell line

Table 4: Structural parameters calculated for azo ligand and its metal complexes.

Bond angles (°)	HL	Selected bond	Cu(II)L	Co(II)L	Fe(II)L
C9-C7-N28	123.62	C9-C7-N29	120.75	120.92	120.05
C7-N28-N27	132.34	C7-N29-N28	114.75	115.04	117.85
C17-N27-N28	131.13	C18-N28-N29	123.56	122.89	122.35
N19-H34-H35	118.14	N20-H35-H51	107.54	106.38	109.47
C36-O37-H45	109.47	C39-O40-H50	114.24	113.71	110.46
O37-C36-O38	109.80	O41-C39-O40	113.19	111.11	118.04
C17-C16-N19	123.39	C17-C18-N20	126.88	125.37	126.95
C14-C16-N19	129.88	C15-C17-N20	127.06	127.36	125.18
C13-C9-C36	116.37	N20-M-Cl43	82.62	80.37	78.36
		C39-O40-M	117.94	116.28	111.39
		O40-M-N20	163.72	164.02	158.63
		N29-M-N20	99.53	96.79	99.53
		Cl-M-N29	176.39	175.64	174.39
Bond lengths (Å)					
C6-C7	1.46	C6-C7	1.43	1.45	1.42
C17-N27	1.40	C18-N28	1.39	1.35	1.36
C7-N28	1.40	C7-N29	1.46	1.43	1.41
N19-H34	1.01	N20-H35	1.00	1.01	1.01
N19-H35	1.01	N20-H39	1.00	1.01	1.01
N27-N28	1.25	N28-N29	1.33	1.35	1.48
C16-N19	1.23	C17-N20	1.46	1.45	1.44
C16-N19	1.32	C17-N20	1.46	1.45	1.44
C9-C36	1.46	C9-N40	1.47	1.48	1.48
C36-O37	1.36	C36-O41	1.39	1.42	1.37
C16-C17	1.34	C17C18	1.42	1.43	1.41
O38-C36	1.22	N20-M	1.92	1.91	1.90
O37-H45	0.96	O40-M	1.96	1.97	2.08
		N29-M	1.90	1.92	1.83

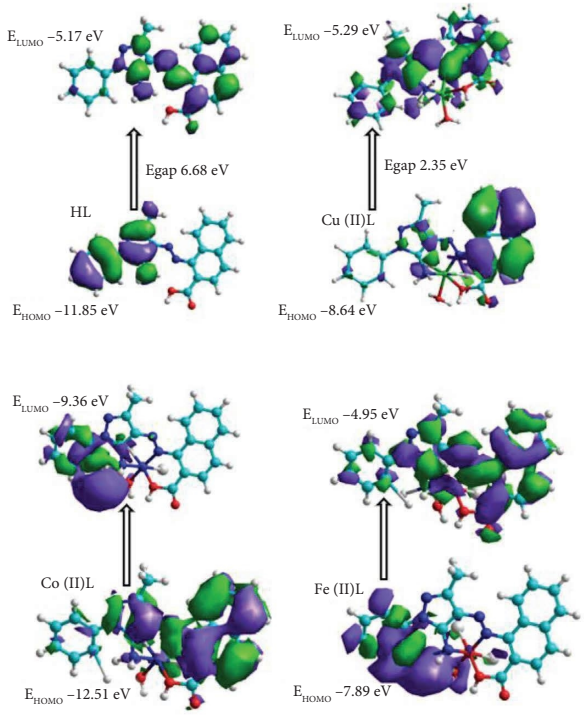

Figure 9: The charge density maps of HOMO and LUMO maps of the studied ligand and its complexes.

(HepG2) using the MTT assay. The IC_{50} (concentration inhibiting 50% of cell proliferation) was determined. The IC_{50} values showed the higher activity of metal complexes at 37°C for 24 h, this may be attributed to the high kinetic stability of the complexes in the growth medium [39]. A microscopy study exposed to different concentrations was recorded and is shown in Figure 11. The results show that the cytotoxic effect of all investigated compounds is higher than that of the cisplatin reference drug. The IC_{50} value against HepG2 of the free ligand is greater than that of all metal complexes, which exhibit low IC_{50} values and greater anticancer agent properties. This high cytotoxicity may be attributed to the increase in conjugation of the ligand moiety on complexation [40, 41]. Moreover, the type of metal ion may affect different cytotoxic properties, which follows the sequence of trends: Co(II)L > Fe(II)L > Cu(II) L > HL > cisplatin on HepG2. According to the toxicity level, a proton coupled electron transfer reaction results in the formation of a resonance stabilized carboxyl radical, which is how compounds based on naphthoic acid exhibit antioxidant activity. By enhancing the resonance stabilized structure's stability and increasing the electron donating effect, substituents can increase the activity of these compounds [42]. The cell viability value of HepG2 was evaluated by the MTT assay, as presented in Figure 12 and Table 7.

Table 5: E_{HOMO}, E_{LUMO}, E_{gap}, and quantum parameters for the HL ligand and its complexes.

Compound	E_{HOMO} (eV)	E_{LUMO} (eV)	E_{gap} (eV)	η (eV)	χ (eV)	S $(eV)^{-1}$	μ (eV)	ω (eV)
HL ligand	−11.85	−5.17	6.68	3.34	8.51	0.14	−8.51	10.84
[Cu(II)L]	−8.64	−5.29	2.35	1.17	11.28	0.42	−6.96	20.61
[Co(II)L]	−12.51	−9.36	3.15	2.57	10.93	0.31	−10.93	37.92
[Fe(II)L]	−7.89	−4.95	2.94	1.47	6.42	0.34	−6.42	14.01

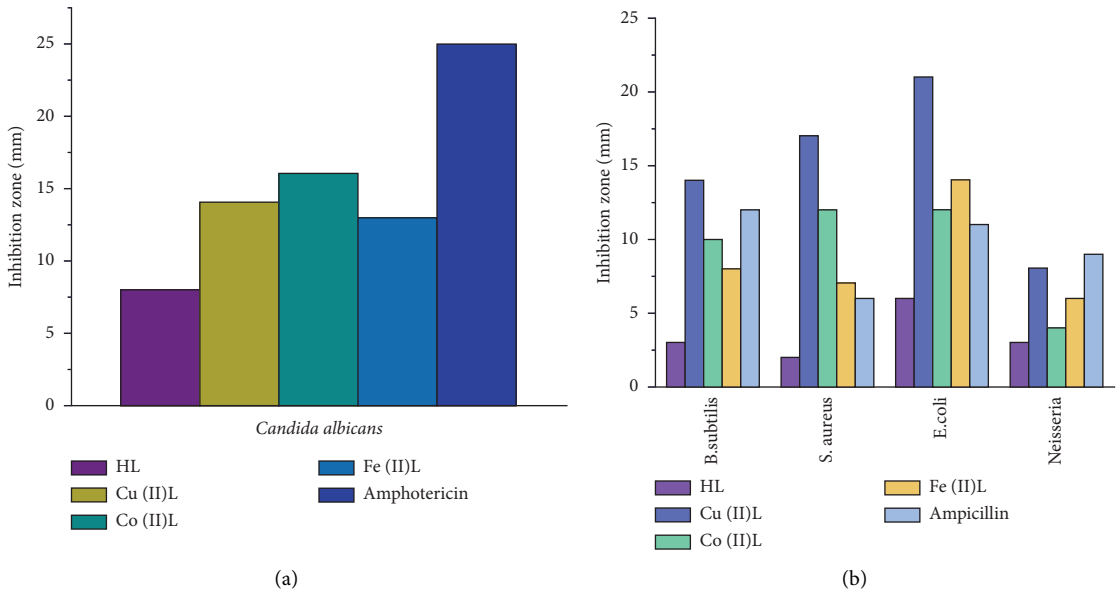

Figure 10: In vitro. (a) Antifungal and (b) antibacterial properties of the azo ligand (HL) and its metal complexes at a concentration of 100 μL.

Table 6: Antibacterial activity data (zone of inhibition in mm) of the ligand and its metal complexes at a concentration of 100 μL.

Complex	Inhibition zone diameter (mm)				
	Gram positive		Gram negative		Fungus
	Bacillus subtilis	*Staphylococcus aureus*	*Escherichia coli*	*Neisseria gonorrhoeae*	*Candida albicans*
Control	—	—	—	—	—
Azo dye ligand	3	2	6	3	8
[Cu(II)L]	14	17	21	8	14
[Co(II)L]	10	12	12	4	16
[Fe(II)L]	8	7	14	6	13
Ampicillin	26	21	25	10	—
Amphotericin	—	—	—	—	25

5.4. DNA Fragmentation Study. The DPA assay is a highly useful tool in quantitatively measuring apoptosis by determining the percentage. The free ligand HL and its Cu(II), Co(II), and Fe(II) complexes exhibited good antioxidant activity; hence, we performed DNA fragmentation analysis. The data on the percentage of fragmentation are displayed in Figure 13 and Table 8. Compared with the large dose, the damage level dramatically decreased when utilizing the 0.1 value, although it was still much higher than in the control group for 24 h. HepG2 was treated with the HL ligand and its Cu(II), Co(II), and Fe(II) complexes, with a percentage of fragmentation of 41.33% (control, 7.00) at $IC_{50} = 22.17$ μg/mL, 42.34% (control, 7.17) at $IC_{50} = 22.09$, 45.36% (control, 7.68) at $IC_{50} = 19.55$ μg/mL, and 43.68% (control, 7.40) at $IC_{50} = 20.16$ μg/mL, respectively. This finding may suggest that the free ligand and its complexes may be considered as a cytotoxic drug by inducing cancer cell death due to DNA damage [43].

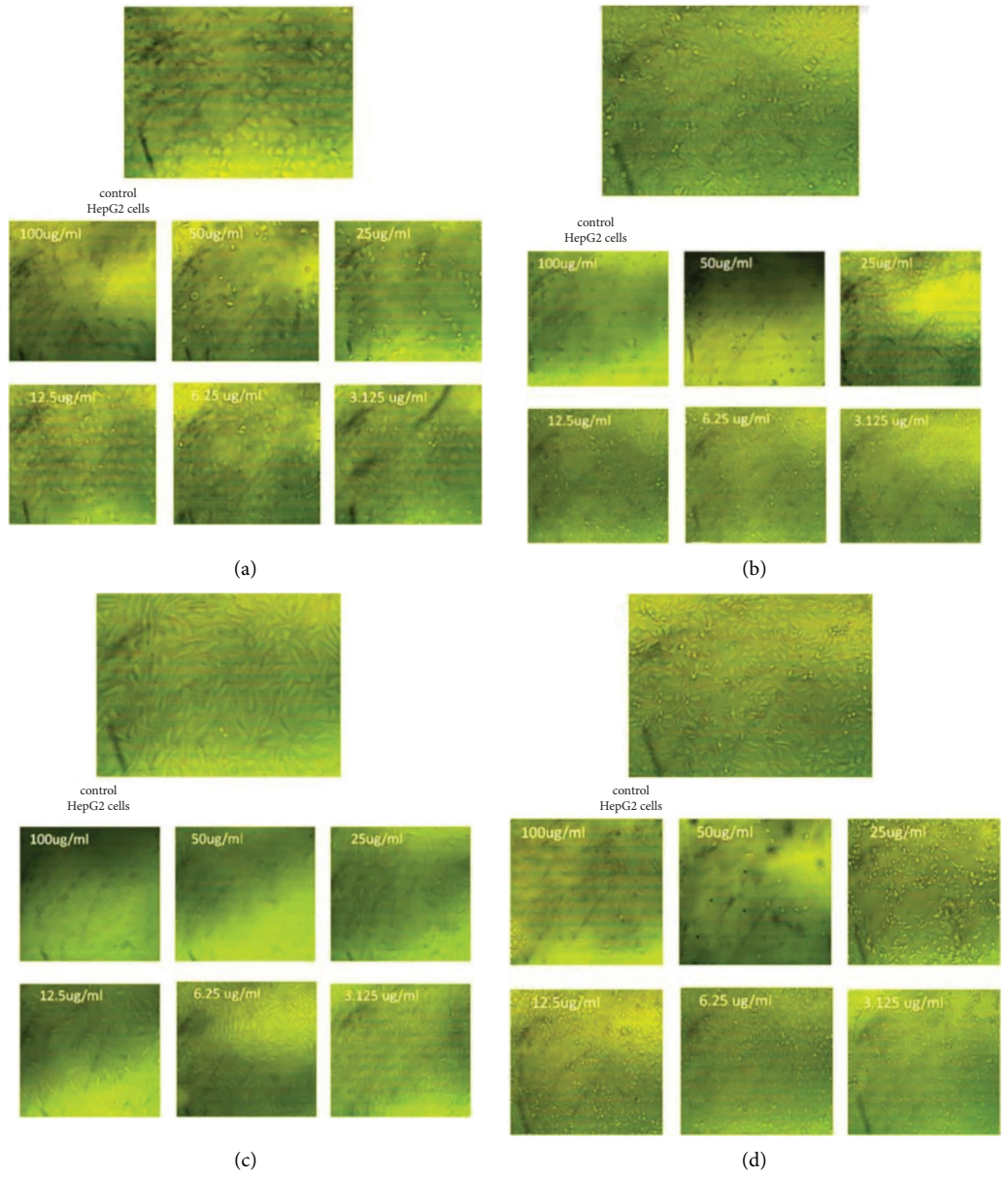

Figure 11: Morphological changes in liver cancer cells (HepG2) treated with different concentrations of (a) ligand and (b) Cu(II), (c) Co(II) and (d) Fe(II) complexes for 24 h.

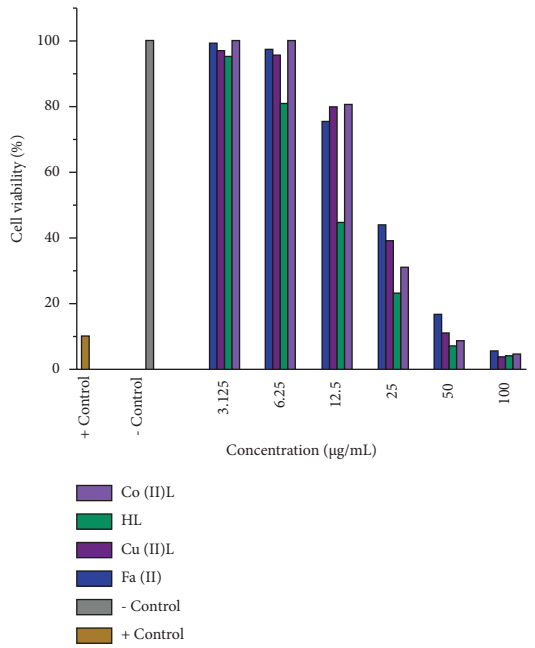

Figure 12: The percentage of the cell viability calculated using the MTT assay in liver cancer cells (HepG2) for the azo dye ligand (HL) and its Cu(II), Co(II), and Fe(II) complexes after 24 h of incubation at various concentrations compared with the positive and negative controls.

Table 7: DNA fragmentation of (a) azo ligand and its (b) Cu(II), (c) Co(II), and (d) Fe(II) complexes at (0.1, 1 μg/mL) on HepG2 cells.

(a)

ID	Conc (μg/ml)	Mean O.D	ST.E	Viability%	Toxicity%	IC_{50}
HL	1 : 02	0.38399	0.0085103	100	0	22.17
	100	0.02198	0.0004462	4.37	112.1860941	
	50	0.06503	0.0068768	7.32	98.92331289	
	25	0.16882	0.0147266	23.32	66.67893661	
	12.5	0.28997	0.0085572	44.84	29.08077709	
	6.25	0.37350	0.0055971	81.04	3.041922291	
	3.125	0.38091	0.0046632	94.99	0.851738241	

(b)

ID	Conc (μg/ml)	Mean O.D	ST.E	Viability%	Toxicity%	IC_{50}
Cu(II)L	1 : 02	0.55468	0.0087534	100	0	22.09
	100	0.0232	0.0011818	4	114.0311	
	50	0.06514	0.0062055	11.24	105.0198	
	25	0.22697	0.0112734	39.16	70.15357	
	12.5	0.463193	0.0067589	79.92	19.53857	
	6.25	0.55295	0.0140606	95.41	0.42109	
	3.125	0.56232	0.0089672	97.03	0.084218	

(c)

ID	Conc (μg/ml)	Mean O.D	ST.E	Viability%	Toxicity%	IC_{50}
Co(II)L	1 : 02	0.46506	0.008486	100	0	19.55
	100	0.02118	0.007632	4.55	113.5772	
	50	0.03548	0.004308	8.9	109.962	
	25	0.11296	0.007851	31.12	90.07848	
	12.5	0.2172	0.005489	80.68	63.36624	
	6.25	0.39255	0.006671	99.94	18.57806	
	3.125	0.46008	0.009135	99.07	0.92827	

(d)

ID	Conc (μg/ml)	Mean O.D	ST.E	Viability%	Toxicity%	IC_{50}
Fe(II)L	1 : 02	0.57501	0.0054149	100	0	20.16
	100	0.02118	0.0004462	5.72	113.293239	
	50	0.03548	0.0027175	16.93	108.4284591	
	25	0.11296	0.0090329	43.96	81.85927673	
	12.5	0.2172	0.0106731	75.51	23.1077044	
	6.25	0.39255	0.0060420	97.26	0	

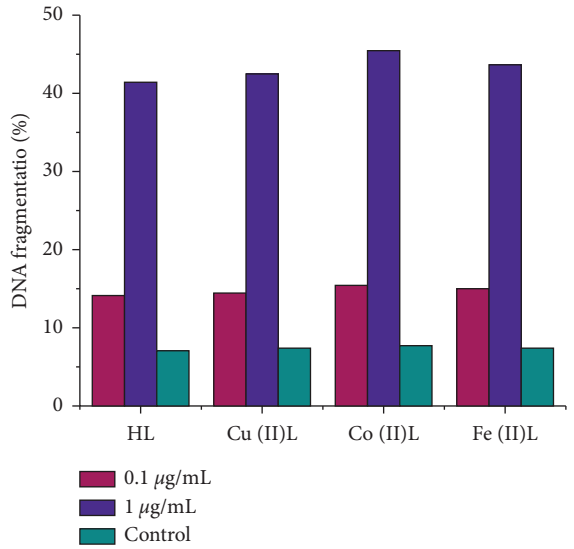

Figure 13: Quantitative estimation of DNA fragmentation % by the diphenylamine assay at various concentrations.

Table 8: DNA fragmentation of (a) azo ligand and its (b) Cu(II), (c) Co(II), and (d) Fe(II) complexes at (0.1, 1 μg/mL) on HepG2 cells.

(a)					
Groups	DNA fragmentation%	SD	P1 Student's *t*-test	P2 Student's *t*-test	Test of significance
HepG2 treated with 0.1 μg/mL	14.100228	1.255707	0.001*	<0.001*	ANOVA $F = 560.109$ $^*P < 0.001$
HepG2 treated with 1 μg/mL	41.332428	1.830609	<0.001*		
Control group	7.004727	0.574902			
(b)					
Groups	DNA fragmentation%	SD	P1 Student's *t*-test	P2 Student's *t*-test	Test of significance
HepG2 treated with 0.1 μg/mL	14.444136	1.286334	0.001*	<0.001*	ANOVA $F = 560.109$ $^*P < 0.001$
HepG2 treated with 1 μg/mL	42.340536	1.875258	<0.0010*		
Control group	7.175574	0.588924			
(c)					
Groups	DNA fragmentation%	SD	P1 Student's *t*-test	P2 Student's *t*-test	Test of significance
HepG2 treated with 0.1 μg/mL	15.47586	1.378215	0.001*	<0.001*	ANOVA $F = 560.109$ $^*P < 0.001$
HepG2 treated with 1 μg/mL	45.36486	2.009205	<0.0010*		
Control group	7.688115	0.63099			
(d)					
Groups	DNA fragmentation%	SD	P1 Student's *t*-test	P2 Student's *t*-test	Test of significance
HepG2 treated with 0.1 μg/mL	14.90268	1.32717	0.001*	<0.001*	ANOVA $F = 560.109$ $^*P < 0.001$
HepG2 treated with 1 μg/mL	43.68468	1.93479	<0.0010*		
Control group	7.40337	0.60762			

P1: comparison of both study groups versus the control group. P2: comparison between both the study groups; $^*P$ is significant at <0.05.

6. Conclusion

A new synthesized HL (1-((5-amino-3-methyl-1-phenyl-*1H*-pyrazol-4-yl) diazenyl)-2-naphthoic acid) and its Cu(II), Co(II), and Fe(II) complexes were prepared and characterized by elemental analysis (H, C, N, and M), spectroscopic analysis (FT-IR, ^{1}H NMR, and UV-vis), and TGA-DTA, which provide good results in thermal stability. The molar conductance values confirmed that all complexes are non-electrolytes and have octahedral geometry. XRD and electron microscopy (SEM) approved that the metal complexes have different morphologies and free ligand. DFT calculations indicate that the high stability of the synthesis compounds depends on Eg values. The in vitro antibacterial and antifungal activities were evaluated, and the results showed poor antimicrobial activity for the free azo ligand against the tested strains, whereas its metal complexes exhibited good to moderate antibacterial and antifungal activities. The new ligand and its complexes were evaluated as cytotoxic candidates against HepG2 through the MTT assay. The Co(II) complex is more biologically effective than the other compounds against the tested cell line, with $IC_{50} = 19.55\ \mu g/mL$. DNA fragmentation and cell death in human liver cancer cells were determined by DPA assay, and the data revealed that the fragmentation percent of each compound increased ca. by 6.5 fold compared with the control cells for 24 h. This result shows the possible application of the investigated compounds as antitumor drugs against human liver cancer cells with further detailed studies and additional verification.

Data Availability

The data used to support the findings of this study are available from the authors upon reasonable request.

Conflicts of Interest

The authors declare that they have no conflicts of interest.

Authors' Contributions

Albandari Alkurdi conceived and designed the experiments, performed the experiments, and wrote the paper. Mutlaq AlJahdali and Abdulmohsen Alshehri revised the paper.

References

[1] R. F. Costa, L. C. Turones, K. V. N. Cavalcante et al., "Heterocyclic compounds: pharmacology of pyrazole analogs from rational structural considerations," *Frontiers in Pharmacology*, vol. 12, Article ID 666725, 2021.

[2] H. Hajati, "Application of organic acids in poultry nutrition," *International International Journal of Avian & Wildlife Biology*, vol. 3, no. 4, pp. 324–329, 2018.

[3] J. J. Max and C. Chapados, "Infrared spectroscopy of aqueous carboxylic Acids: comparison between different acids and their salts," *The Journal of Physical Chemistry A*, vol. 108, pp. 3324–3337, 2004.

[4] V. Uivarosi, "Metal complexes of quinolone antibiotics and their applications: an update," *Molecules*, vol. 18, pp. 11153–11197, 2013.

[5] A. K. Sarangi, B. B. Mahapatra, R. K. Mohapatra et al., "Synthesis and characterization of some binuclear metal complexes with a pentadentate azodye ligand: an experimental and theoretical study," *Applied Organometallic Chemistry*, vol. 34, no. 8, p. 5693, 2020.

[6] K. Cai, H. He, Y. Chang, and W. Xu, "An Efficient and Green Route to Synthesize Azo Compounds through Methyl Nitrite," *Green and Sustainable Chemistry*, vol. 4, 2014.

[7] N. M. Aljamali, "Review in azo compounds and its biological activity," *Biochemistry & Analytical Biochemistry*, vol. 04, no. 02, pp. 1–4, 2015.

[8] G. Ciçen, C. Karabacak Atay, and T. Tilki, "Disazo dyes containing pyrazole and benzothiazole moieties: synthesis, characterization, absorption characteristics and tautomeric structures," *Research on Chemical Intermediates*, vol. 43, no. 12, pp. 6803–6816, 2017.

[9] H. Kyhoiesh and K. Al-Adilee, "Synthesis, spectral characterization, antimicrobial evaluation studies and cytotoxic activity of some transition metal complexes with tridentate (N,N,O) donor azo dye ligand," *Results in Chemistry*, vol. 3, Article ID 100245, 2021.

[10] K. Al-Adilee, A. Abass, and A. Taher, *Journal of Molecular Structure*, vol. 1108, pp. 378–397, 2016.

[11] A. Bauer, *American Journal of Clinical Pathology*, vol. 45, pp. 149–158, 1966.

[12] M. J. Matar, L. Ostrosky-Zeichner, V. L. Paetznick, J. R. Rodriguez, E. Chen, and J. H. Rex, "Correlation between E-test, disk diffusion, and microdilution methods for antifungal susceptibility testing of fluconazole and voriconazole," *Antimicrobial Agents and Chemotherapy*, vol. 47, pp. 1647–1651, 2003.

[13] L. D. Liebowitz, H. Ashbee, E. V. Evans et al., "A two year global evaluation of the susceptibility of Candida species to fluconazole by disk diffusion," *Diagnostic Microbiology and Infectious Disease*, vol. 40, no. 1-2, pp. 27–33, 2001.

[14] T. Slater, B. Sawyer, and U. Sträuli, "Studies on succinate-tetrazolium reductase systems," *Biochimica et Biophysica Acta*, vol. 77, pp. 383–393, 1963.

[15] A. Gaber, W. F. Alsanie, D. N. Kumar, M. S. Refat, and E. M. Saied, "Novel papaverine metal complexes with potential anticancer activities," *Molecules*, vol. 25, no. 22, p. 5447, 2020.

[16] A. Bouslimi, C. Bouaziz, I. Ayed-Boussema, W. Hassen, and H. Bacha, "Individual and combined effects of ochratoxin A and citrinin on viability and DNA fragmentation in cultured Vero cells and on chromosome aberrations in mice bone marrow cells," *Toxicology*, vol. 251, no. 1-3, pp. 1–7, 2008.

[17] F. Marotta, H. Yadav, U. Gumaste, A. Helmy, S. Jain, and E. Minelli, "Protective effect of a phytocompound on oxidative stress and DNA fragmentation against paracetamol-induced liver damage," *Annals of Hepatology*, vol. 8, no. 1, pp. 50–56, 2009.

[18] F. K. Ommenya, E. A. Nyawade, D. M. Andala, and J. Kinyua, "Synthesis, characterization and antibacterial activity of Schiff base, 4-Chloro-2-{(E)-[(4-fluorophenyl) imino] methyl} phenol metal (II) complexes," *Journal of Chemistry*, vol. 2020, pp. 1–8, Article ID 1745236, 2020.

[19] P. Debnath, A. Das, K. S. Singh et al., "Synthesis, structural characterization and antimicrobial activities of tri-organotin(IV)azo-carboxylates derived from ortho/para-

amino benzoic acids and β-naphthol," *Inorganica Chimica Acta*, vol. 498, Article ID 119172, 2019.

[20] M. Shakir, N. Begum, Y. Azim, and S. Parveen, "Synthesis of 14-Membered Pentaazabis(Macrocyclic) Complexes of Co(II), Ni(II), Cu(II), and Zn(II) Derived from Hydrazine and Their Physico-chemical Studies," *Synthesis and Reactivity in Inorganic and Metal-organic Chemistry*, vol. 8, pp. 1367–1379, 2003.

[21] W. H. Mahmoud, R. G. Deghadi, and G. G. Mohamed, "Spectroscopic and thermal characterization of biologically and anticancer active novel Schiff base metal complexes," *Research on Chemical Intermediates*, vol. 42, no. 12, pp. 7869–7907, 2016.

[22] D. Gürbüz, A. Çinarli, A. Tavman, and A. S B Tan, "Synthesis, characterization and antimicrobial activity of some transition metal complexes of N-(5-chloro-2-hydroxyphenyl)-3-methoxy-salicylaldimine," *Bulletin of the Chemical Society of Ethiopia*, vol. 29, pp. 63–74, 2015.

[23] A. Jarad and Z. Kadhim, *Int. J. Human. Arts. Med. Sci.*vol. 3, pp. 197–210, 2015.

[24] A. Osowole, O. Agbaje, and S. Wakil, *Int. J. Appl. Med. Sci.*vol. 2, pp. 77–87, 2015.

[25] E. Yildiz and H. Boztepe, *Turkish Journal of Chemistry*, vol. 26, pp. 897–904, 2002, https://journals.tubitak.gov.tr/chem/vol26/iss6/11.

[26] A. El Tabl, M. Abd Wlwahed, M. Abd-Elwareth, and S. Faheem, "Schiff-base, Egypt," *Journal of Chemistry*, vol. 64, pp. 3131–3152, 2021.

[27] M. H. Nair and A. Appukuttan, "Syntheses, spectral, surface morphological and gamma ray irradiation studies of some oxomolybdenum(V) and dioxomolybdenum(VI) complexes of an azo dye derived from 4-aminoantipyrine," *Journal of the Korean Chemical Society*, vol. 56, no. 2, pp. 217–227, 2012.

[28] E. Ispir, "The synthesis, characterization, electrochemical character, catalytic and antimicrobial activity of novel, azo-containing Schiff bases and their metal complexes," *Dyes and Pigments*, vol. 82, pp. 13–19, 2009.

[29] B. Ravi, J. Keshavayya, N. Mallikarjuna, and H. Santhosh, "Synthesis, characterization, cyclic voltammetric and cytotoxic studies of azo dyes containing thiazole moiety," *Chemical Data Collections*, vol. 25, p. 100334, 2020.

[30] A. Bartyzel, "Synthesis, thermal behaviour and some properties of CuII complexes with N, O-donor Schiff bases," *Journal of Thermal Analysis and Calorimetry*, vol. 131, no. 2, pp. 1221–1236, 2018.

[31] U. Holzwarth and N. Gibson, "The Scherrer equation versus the 'Debye-Scherrer equation'," *Nature Nanotechnology*, vol. 6, p. 534, 2011.

[32] R. H. Abu-Eittah and W. A. Zordok, "A molecular orbital treatment of piroxicam and its M2+-complexes: the change of the drug configuration in a time of bond formation," *Journal of Molecular Structure: THEOCHEM*, vol. 951, no. 1-3, pp. 14–20, 2010.

[33] E. C. Agwamba, A. D. Udoikono, H. Louis et al., "Synthesis, characterization, DFT studies, and molecular modeling of azo dye derivatives as potential candidate for trypanosomiasis treatment," *Chemical Physics Impact*, vol. 4, p. 100076, 2022.

[34] A. F. Alkurdi, M. S. AlJahdali, and A. A. Alshehri, "Synthesis, characterization, DFT calculation, and biological activity of pyrazole-based azo-metal (II) complexes," *Results in Chemistry*, vol. 4, Article ID 100566, 2022.

[35] E. Aljuhani, M. M. Aljohani, A. Alsoliemy et al., "Synthesis and characterization of Cu(II)-pyrazole complexes for possible anticancer agents; conformational studies as well as compatible in-silico and in-vitro assays," *Heliyon*, vol. 7, no. 11, Article ID e08485, 2021.

[36] N. Ganji, V. K. Chityala, P. K. Marri et al., "DNA incision evaluation, binding investigation and biocidal screening of Cu(II), Ni(II) and Co(II) complexes with isoxazole Schiff bases," *Journal of Photochemistry and Photobiology B: Biology*, vol. 175, pp. 132–140, 2017.

[37] Y. Bayeh, A. Abebe, M. Thomas, and W. Linert, "Synthesis, Characterization and Antimicrobial Activities of New Mixed Ligand Complexes of Copper(II) with 1,10-Phenanthroline and Thymine," *Journal of Transition Metal Complexes*, vol. 2, pp. 1–6, 2019.

[38] N. El-Gamel, "Metal chelates of ampicillin versus amoxicillin: synthesis, structural investigation, and biological studies," *Journal of Coordination Chemistry*, vol. 63, pp. 534–543, 2010.

[39] S. A. Elsayed, H. E. Badr, A. di Biase, and A. M. El-Hendawy, "Synthesis, characterization of ruthenium (II), nickel (II), palladium (II), and platinum (II) triphenylphosphine-based complexes bearing an ONS-donor chelating agent: interaction with biomolecules, antioxidant, in vitro cytotoxic, apoptotic activity and cell cycle analysis," *Journal of Inorganic Biochemistry*, vol. 223, Article ID 111549, 2021.

[40] A. M. Khedr, H. El-Ghamry, M. A. Kassem, F. A. Saad, and N. El-Guesmi, "Novel series of nanosized mono- and homobinuclear metal complexes of sulfathiazole azo dye ligand: synthesis, characterization, DNA-binding affinity, and anticancer activity," *Inorganic Chemistry Communications*, vol. 108, p. 107496, 2019.

[41] M. Mokhtari, A. Akbarzadeh, M. Hashemi et al., *Adv Stud Biol*, vol. 1, pp. 19–25, 2012.

[42] N. Venugopal, G. Krishnamurthy, H. Bhojyanaik, and P. Murali Krishna, "Synthesis, spectral characterization and biological studies of Cu (II), Co (II) and Ni (II) complexes of azo dye ligand containing 4–amino antipyrine moiety," *Journal of Molecular Structure*, vol. 1183, pp. 37–51, 2019,

[43] A. Basu and S. Krishnamurthy, "Cellular Responses to Cisplatin-Induced DNA Damage," *Journal of Nucleic Acids*, vol. 2010, Article ID 201367, 2010.